ADVANCED FUNCTIONAL MATERIALS
www.afm-journal.de

Amorphous Zinc Stannate (Zn_2SnO_4) Nanofibers Networks as Photoelectrodes for Organic Dye-Sensitized Solar Cells

Seung-Hoon Choi, Daesub Hwang, Dong-Young Kim, Yann Kervella, Pascale Maldivi, Sung-Yeon Jang, Renaud Demadrille,* and Il-Doo Kim**

A new strategy for developing dye-sensitised solar cells (DSSCs) by combining thin porous zinc tin oxide (Zn_2SnO_4) fiber-based photoelectrodes with purely organic sensitizers is presented. The preparation of highly porous Zn_2SnO_4 electrodes, which show high specific surface area up to 124 m^2/g using electrospinning techniques, is reported. The synthesis of a new organic donor-conjugate-acceptor (D-π-A) structured orange organic dye with molar extinction coefficient of 44 600 M^{-1} cm^{-1} is also presented. This dye and two other reference dyes, one organic and a ruthenium complex, are employed for the fabrication of Zn_2SnO_4 fiber-based DSSCs. Remarkably, organic dye-sensitized DSSCs displayed significantly improved performance compared to the ruthenium complex sensitized DSSCs. The devices based on a 3 μm-thick Zn_2SnO_4 electrode using the new sensitizer in conjunction with a liquid electrolyte show promising photovoltaic conversion up to 3.7% under standard AM 1.5G sunlight (100 mW cm^{-2}). This result ranks among the highest reported for devices using ternary metal oxide electrodes.

1. Introduction

Since the pioneer work of Grätzel and O'Regan in the early 1990s,[1] dye-sensitized solar cells (DSSCs), have attracted increasing attention as third generation photovoltaic (PV) cells due to their convenient and low cost fabrication process, and their relatively high efficiency.[2] The breakthrough in the photoelectric conversion efficiency of DSSCs achieved in the early 1990s is now being intensively pursued and efficiencies as high as 12.3% have been reached within the last years.[2d] Several advances in the design of dyes and electrolytes have led to this record power conversion efficiency (PCE).[3] For improving the performances of DSSCs, many different strategies have been recently explored. One can cite the use of dye antenna, energy relay dyes, and inorganic dyes[3f] or alternatively the development of new oxides or tandem solar cells.[3g] In this work we have combined two approaches by synthesizing new dyes with high molar extinction coefficients and by developing new oxide films with large total surface area and high electron mobility.

Among the materials routinely used for the fabrication of high efficiency DSSC, one can cite the nanostructures made of titanium dioxide. TiO_2 photoelectrodes have been the focus of a tremendous number of studies over the last years.[4] However, more recently new materials have been introduced to replace TiO_2 and efficiently used for the fabrication of DSSC. Previous research has been restricted to binary oxides, including ZnO,[5] SnO_2,[6] Nb_2O_5,[7] and In_2O_3.[8] In contrast, the application of multication oxides has been scarcely investigated. In comparison with simple binary oxides, multication oxides have several strong advantages. By altering their composition, i.e., by varying the relative elements ratio, their band gap energy, work function, and electric resistivity can be readily tuned. Considering the availability of a wide range of multi-cation oxides and their tunable properties, it could be interesting to explore their applications as photo-electrodes in DSSCs with a potential to obtain

Dr. S.-H. Choi
Department of Chemical Engineering
Hanyang University
Seoul 133-791, Republic of Korea
D.-S. Hwang, Dr. D.-Y. Kim
Polymer Hybrid Center
Korea Institute of Science and Technology
P. O. Box 131, Cheongryang, Seoul 130-650, Republic of Korea
Y. Kervella, Dr. R. Demadrille
INAC/SPrAM UMR 5819 CEA-CNRS-Univ.J.Fourier-Grenoble 1
LEMOH, 17 Rue des Martyrs,
38054 Grenoble Cedex 9, France
E-mail: renaud.demadrille@cea.fr

DOI: 10.1002/adfm.201203278

Dr. P. Maldivi
INAC/SCIB UMR E3 CEA- Univ.J.Fourier-Grenoble 1
17 Rue des Martyrs,
38054 Grenoble Cedex 9, France.
Prof. S.-Y. Jang
Department of Chemistry
Kookmin University
Seoul 136-702, Republic of Korea
E-mail: syjang@kookmin.ac.kr
Prof. I.-D. Kim
Department of Materials Science and Engineering
Korea Advanced Institute of Science and Technology
Daejeon 305-701, Republic of Korea
E-mail: idkim@kaist.ac.kr

new materials with better performance than anatase TiO_2. To the best of our knowledge, only two types of ternary oxides, $SrTiO_3$[9] and Zn_2SnO_4,[10] have been reported for the fabrication of photo-electrodes in DSSCs.

Among the multication oxides, zinc stannate (Zn_2SnO_4) is a transparent conducting oxide (TCO) material which could lead to promising performances in DSSCs since it has a band gap of 3.6 eV and an electron mobility up to 15 $cm^2\ V^{-1}\ s^{-1}$.[11] The first example of application of Zn_2SnO_4 in DSSC was reported by Wu and co-workers. In this work, the photoelectrode was fabricated using nanoparticles formed by decomposing a mixture of zinc and tin *ter*-butylamine complexes under hydrothermal conditions.[12] The highest energy conversion efficiency of 4.7% was achieved from a Zn_2SnO_4 cell with 10 μm film thickness employing N719 as sensitizer.[10]

Sensitizing dyes are another key element in high efficiency DSSCs. Although high performances DSSCs have traditionally been fabricated using ruthenium-based complexes,[13] high price due to limited availability of ruthenium on earth, limits the practical and extended industrial application of ruthenium-containing DSSCs. Besides, even though "champion" ruthenium-based complexes, such as N3 or CYC B11, show broad absorption spectra, unfortunately they also have low molar extinction coefficients (< 25 000 M^{-1} cm).[2c,14]

To overcome these barriers, several promising organic dyes specifically designed to be grafted on Zn, Sn, and Ti based oxides, have been synthesized over the past five years.[15] Because of their higher molar extinction coefficients compared to ruthenium based dyes, the thicknesses of the semiconducting oxide layers (and as a consequence the amount of material necessary to fabricate them) can be significantly decreased without reducing the light-harvesting efficiency and the performances of the solar cells.

Here, we propose a new strategy for developing DSSCs by combining thin porous Zn_2SnO_4 fiber-based photoelectrodes prepared via electrospinning (e-spin) with purely organic sensitizers. In this work, the sub-micrometer scale of Zn_2SnO_4 fibers, embedded by nanoscale particles, which are constructed by in situ phase separation between an inorganic precursor $Zn(OAc)_2$-$Sn(OAc)_4$ and polymer matrix, i.e., poly(vinylacetate), enabled the fabrication of efficient DSSCs after sensitization of organic dyes. Three different sensitizers, two donor-conjugate-acceptor (D-π-A) structured organic dyes and a ruthenium complex (N719) dye were used for the fabrication of Zn_2SnO_4 fiber-based DSSCs. For the organic sensitizers, we selected first a dye known as TA-St-CA[16] for which a photoconversion efficiency in DSSCs was demonstrated to be as high as 9% under open-cell conditions (without an aperture mask) and secondly we synthesized an analogue of this dye containing an additional thiophene subunit, abbreviated as TA-TV-CA. The performance of DSSCs using Zn_2SnO_4 fiber photoelectrodes with these three dyes were investigated, and the advantages of thin porous photoelectrodes were discussed. Remarkably, organic dye sensitized DSSCs displayed significantly improved performance compared to the N719 sensitized DSSCs. The optimized (PCE) of TA-TV-CA sensitized cells reaches ca. 3.7% on a 3 μm-thick Zn_2SnO_4 electrode, which is slightly higher than that of TA-St-CA sensitized cells (3.5%) on a 4 μm-thick Zn_2SnO_4 electrode. The PCEs of both organic dyes were ≈2.5 times higher that that of N719 (1.4%). Considering that the best performances of the organic dye are obtained with a relatively low film thickness (<4 μm) of Zn_2SnO_4, the results look promising in the perspective of application to solid-state cells.[17]

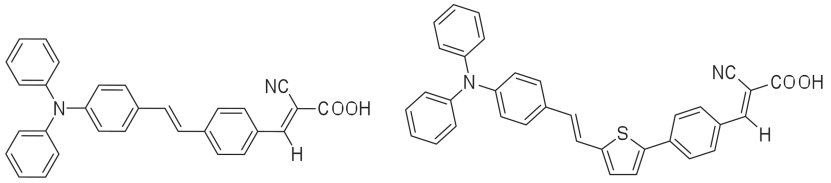

Scheme 1. Chemical structures of organic sensitizers TA-St-CA and TA-TV-CA.

2. Results and Discussion

2.1. Organic Dyes

2.1.1. Design and Synthesis

Scheme 1 shows the chemical structures of organic dyes TA-St-CA and TA-TV-CA that have been prepared in this study. Both dyes contain a tri-phenylamine electron-donating group connected by a π-conjugated spacer to a cyanocarboxylic acid that acts as an electron-accepting group and anchor for the grafting onto the surface of the photoelectrodes.

TA-St-CA dye was first reported by Hwang and co-workers in 2007 and was found to be a highly efficient sensitizer for TiO_2. Using this dye, solar cells showing a short-circuit current density (J_{sc}) of ca 18 mA cm^{-2} were fabricated.[16] It is well known that the J_{sc} of DSSCs is strongly related to the light absorption range of sensitizers. For that reason, we decided in this work to synthesize an analog of TA-St-CA containing an additional thiophene unit in the π-conjugated spacer. The incorporation of electron-rich thiophene ring is expected to enhance the intramolecular charge transfer that occurs in such molecular systems and to result in a bathochromic shift and an increase of the absorption band located in the visible part of the spectrum.

TA-St-CA was prepared in three steps according to published procedures.[16a] **Figure 1** presents the synthetic strategy which has been developed to access TA-TV-CA. This thiophene containing dye was prepared in a very straightforward manner in three steps starting from commercially available compounds such as 4-(thien-2-yl)benzaldehyde. After bromination of the starting material using *N*-bromosuccinimide (NBS), compound **(1)** is obtained in a good yield (71%) and then coupled through a palladium-catalyzed cross-coupling reaction according to Heck conditions to *N*,*N*-diphenyl-4-vinylaniline (TA-Vinyl[16a]). The molecule **(2)** was obtained in 41% yield and this intermediate was then converted in the next step into the expected dye by Knoevenagel condensation reaction. Starting from 4-(thien-2-yl) benzaldehyde the overall yield for the preparation of TA-TV-CA was 20%.

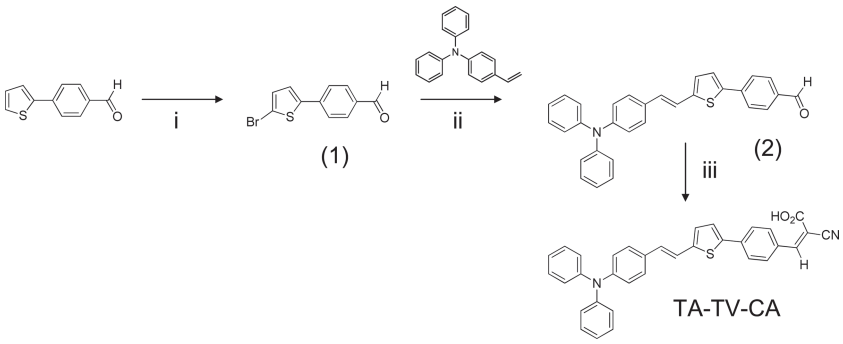

Figure 1. Synthetic route of TA-TV-CA. Reaction conditions: i) NBS, *N*,*N*-dimethylformamide (DMF), methanol (CH_3OH), 0 °C to room temperature, 2 h. ii) Trans-di(μ-acetato)bis[o-(di-o-tolylphosphino)benzyl] dipalladium(II), 2,6-di-tert-butylcresol, Na_2CO_3, N,N-dimethylacetamide (DMAc), 135 °C, 24 h. iii) Cyano-acrylic acid, acetonitrile (ACN), few drops of pyridine, reflux, 2 h.

2.1.2. Optical and Electrochemical Properties

The UV-Vis absorption spectra of TA-St-CA and TA-TV-CA in dilute ethanol solution are shown in **Figure 2**. As expected, the thiophene-containing dye TA-TV-CA shows an absorption band that is red-shifted by 20 nm compared to its analog. The red shift of the maximum wavelength of absorption and the onset is caused by the increase of the conjugation length of the π-conjugated bridge due to the incorporation of the thiophene unit. In addition to the shift and the broadening of the absorption spectrum, the molar extinction coefficient at the maximum absorption wavelength of this dye is strongly increased compared to TA-St-CA ($\varepsilon = 36\ 100\ M^{-1}cm^{-1}$) and reaches $\varepsilon = 44\ 600\ M^{-1}cm^{-1}$ in ethanol. It should be noted that the molar extinction coefficient of the new dye is almost two times higher than the ones of most of ruthenium complex photosensitizers[18] and three times higher than the one of N719.[14]

To investigate the molecular energy levels of the dyes and to evaluate the possibility of electron transfer from the excited state of the dye molecules to the conduction band (CB) of Zn_2SnO_4 and from the electrolyte to the oxidized molecules, electrochemical experiments were carried out. The highest occupied molecular orbital (HOMO) energy levels of the organic dyes were estimated from the onset of their oxidation potentials by using cyclic voltammetry. TA-St-CA and TA-TV-CA showed quasi reversible oxidation waves at 0.40 V and 0.30 V, respectively (vs. Fc^+/Fc), whereas their reduction waves were found to be irreversible. Therefore, the lowest unoccupied molecular orbital (LUMO) energy levels of the dyes were calculated from the HOMO values and the optical band gap estimated from the absorption edge of their absorption spectra. The optical data, the HOMO-LUMO energy levels positions and band gap energies are summarized in **Table 1**.

The results obtained for TA-St-CA are in good accordance with those reported previously.[16] As expected, we found that the incorporation of a thiophene unit in the dye structure results in the rise of the HOMO energy level by 0.1 eV. The HOMO energy level position of TA-TV-CA is located at –5.10 eV while the one of TA-St-CA is at –5.20 eV. The LUMO energy level position seems not to be affected and is found at –2.70 eV for both dyes.

The experimental values were compared to those obtained from density functional theory (DFT) calculations and were found relatively similar with deviations of less than 0.3 eV. We report in **Figure 3** the calculated molecular orbital energy diagram for TA-St-CA and TA-TV-CA, along with *iso* density plots of the HOMO and LUMO. The dyes show a directional electron distribution, with the delocalization of the HOMO on the triphenylamino group and the π-conjugated bridge. The LUMO of both dyes were predominantly delocalized on the phenylvinylcyanoacetic units. This electron distribution should facilitate the reduction of the oxidized dyes by the electrolyte and favor the injection of electrons into the Zn_2SnO_4 electrodes.

From the experimental and theoretical data we can conclude that the energy levels positions of both dyes provide a favorable matching with the CB of Zn_2SnO_4 (located around –3.9 eV vs. vacuum)[11] and from the redox level of the I_3^-/I^- based electrolyte, which is situated at –4.83 eV vs. vacuum.[3f]

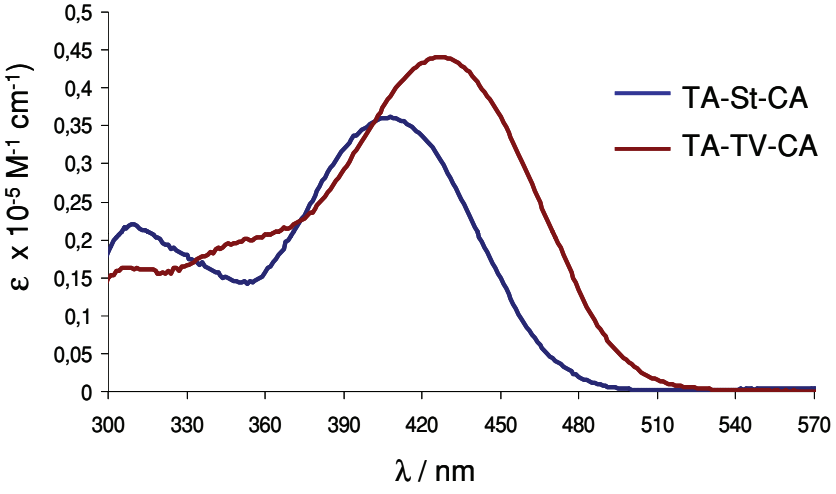

Figure 2. Absorption spectra of TA-St-CA and TA-TV-CA in ethanol (10^{-5} M).

2.2. Preparation and Characterization of the Zn_2SnO_4 Fiber-based Electrodes

2.2.1. Preparation of the Zn_2SnO_4 Fibers

The Zn_2SnO_4 fibers were synthesized by e-spinning a zinc acetate/tin acetate/poly(vinylacetate) (PVAc) solution in DMF using a single spinneret. **Figure 4**a–d presents microstructures of electrospun zinc stannate fibers obtained after heating from 450 °C to 700 °C for 1 h. The as-spun $Zn(OAc)_2$-$Sn(OAc)_4$/PVAc composite nanofibers exhibit randomly oriented fibers in the form of

Table 1. Optical and electrochemical properties of TA-St-CA, TA-TV-CA and N719.[3f]

Dye	λ max [nm]	ε [M^{-1} cm^{-1}]	HOMO[a)] [eV]	LUMO[b)] [eV]	E_g[c)] [eV]	HOMO^{Calc} [eV]	LUMO^{Calc} [eV]
TA-St-CA	407	36 100	–5.20	–2.70	2.50	–5.31	–3.01
TA-TV-CA	427	44 600	–5.10	–2.70	2.40	–5.15	–3.01
N719[d)]	535	13 500	–5.38	–3.06	2.32	–	–

[a)]Estimated from the oxidation potential, determined by cyclic voltametry (HOMO vs. $Fc^+/Fc_{(vac)}$ = –4.8 V); [b)]Estimated from the edge of the absorption spectrum. Calculated from the band gap and the HOMO value; [c)]Estimated from the edge of the absorption spectrum; [d)]See ref. [3f]

nonwoven mats with diameters ranging from 380 to 752 nm and lengths of several hundred micrometers (Figure 4a). Calcination of the composite fibers at 450 °C resulted in the formation of Zn_2SnO_4 fibers as a result of the decomposition of PVAc matrix. Diameters of Zn_2SnO_4 fibers ranged from 352 to 705 nm. During calcinations step, slight shrinkage was observed due to the densification of the Zn_2SnO_4 fibers.

2.2.2. Structural Characterization of the Zn_2SnO_4 Fibers

Figure 4a shows surface morphology of as-spun $Zn(OAc)_2$-$Sn(OAc)_4$/PVAc composite fibers in the diameter range of 300–800 nm. After calcination at 450 °C, Zn_2SnO_4 fibers with relatively rough surface morphology were prepared after thermal decomposition of PVAc. In order to clearly examine the microstructural evolution of the inner morphology of porous Zn_2SnO_4 fibers, we conducted focused ion beam (FIB)-SEM analyses on a single Zn_2SnO_4 fiber. Figure 4c shows the longitudinal and cross-sectional images of FIB-cut Zn_2SnO_4 fiber calcined at 450 °C. The surface and inner morphology of the fibers are highly porous and smooth. On the contrary, as the calcination temperature increased up to 700 °C, Zn_2SnO_4 fibers crystallized into inverse spinel Zn_2SnO_4 phase with rougher surface structures retaining its highly porous surface and inner morphology (Figure 4d). The high porosity is originated from phase separation between PVAc polymer and inorganic salts. Polymer (PVAc) rich region is converted into voids after calcinations at 700 °C while inorganic precursor rich region is converted into polycrystalline Zn_2SnO_4 solid fibers. Detailed morphological characteristics are described in our previous work.[19]

Calcined metal oxide fibers often suffer from poor adhesion to the substrates. In the case of Zn_2SnO_4 fibers, after calcination at 450 °C, the fibers can peel off from the substrate. To overcome this problem, we introduced a thermo-compression step to drive better adhesion of the PVAc matrix that has relatively low glass transition temperature (30–40 °C), onto FTO-coated glass substrate prior to calcination procedure. After the thermo-compression and subsequent heat treatment, the Zn_2SnO_4 fibers were not peeled off from the substrate during the rest of cell fabrication process. Interestingly, well-interconnected fused morphologies of the Zn-Sn precursor/PVAc composite fibers were obtained due to the partial welding of the PVAc (Figure 4e). Subsequent calcination at 450 °C for 1 h in air resulted in a highly porous network structure (see Figure 4f) with high specific surface area of 124 m^2/g determined using the Brunauer-Emmett-Teller (BET) method. It should be noted that this value is the highest ever reported for Zn_2SnO_4 electrode. The inset image of Figure 4f emphasizes that the Zn_2SnO_4 fibers are composed of nanoparticles of less than 5 nm in diameter. Figure 4g shows FIB-cut cross-sectional image of Zn_2SnO_4 fibers calcined at 450 °C. The thickness was 3 μm and a highly porous structure was observed. The smaller pores were found at the interior of the Zn_2SnO_4 fibers while the large pores appeared at macroporous regions separating the individual fibers. The unique structural features with bimodal pore size distribution are very advantageous, providing high porosity for efficient permeability of dye-solution and electrolytes into the inner fibers while maintaining a high surface area for enhanced surface photosensitization.

In order to determine the microstructure and for phase identification of Zn_2SnO_4 fibers in greater detail, we carried out high-resolution transmission electron microscopy (HR-TEM) analysis (Figure 4h–j). Figure 4h shows TEM images of randomly distributed Zn_2SnO_4 fibers with diameters in the range of 350–700 nm. The image indicates that the surface of the Zn_2SnO_4 fibers is relatively

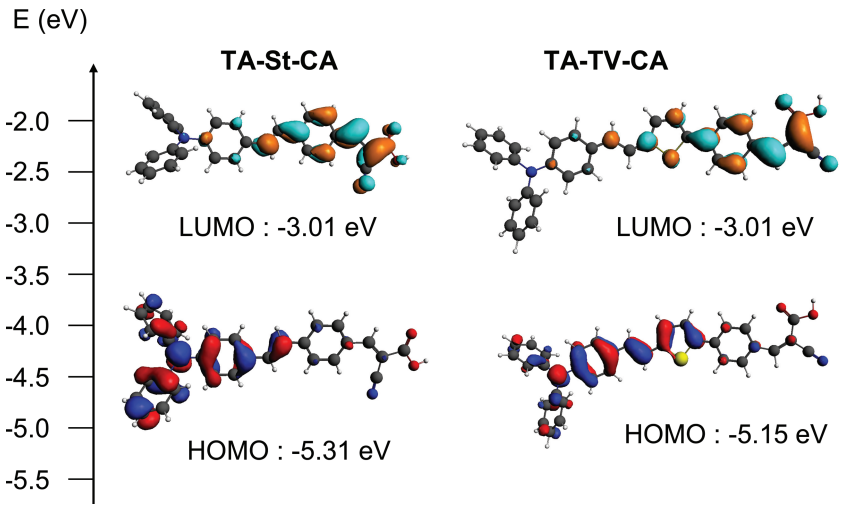

Figure 3. Frontier orbitals (HOMO and LUMO) of TA-St-CA and TA-TV-CA optimized with DFT at the B3LYP/TZ2P level.

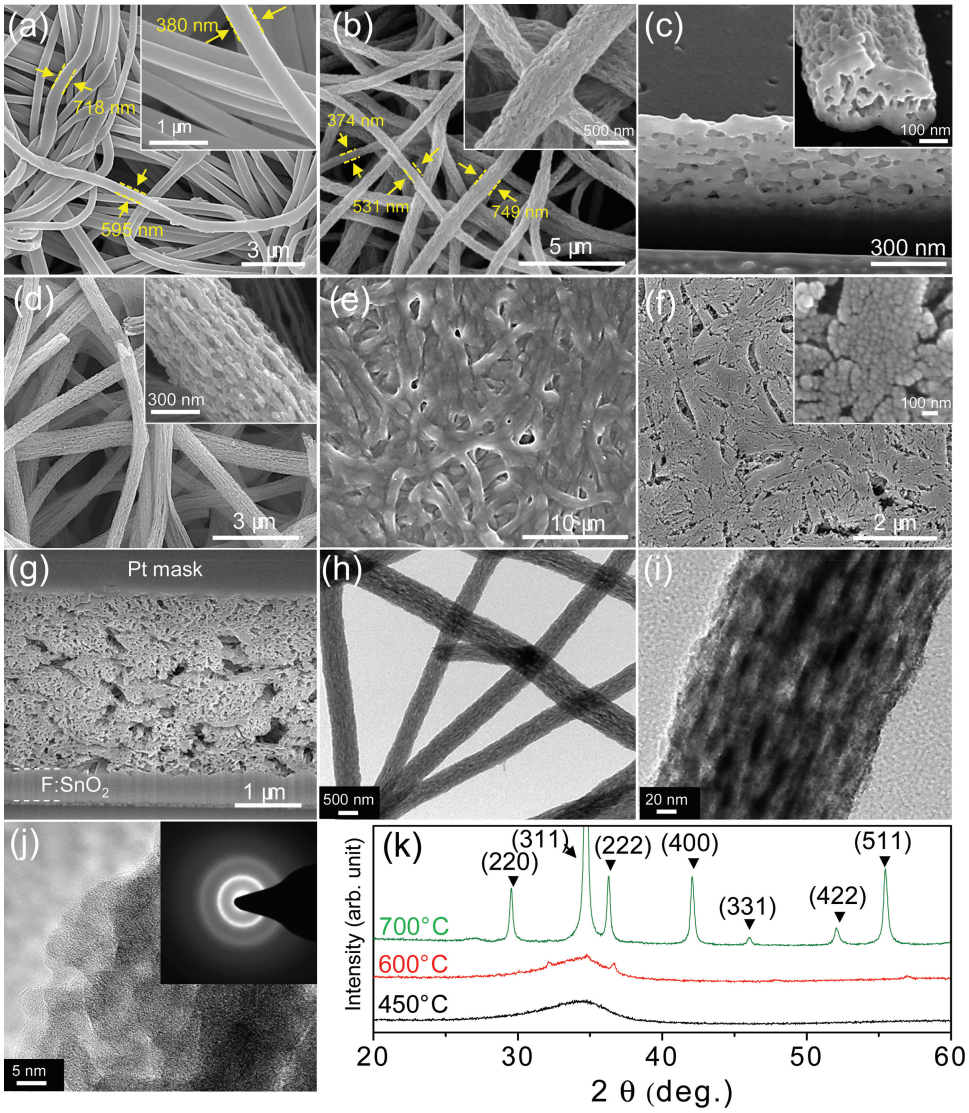

Figure 4. a) SEM image of as-spun $Zn(OAc)_2$-$Sn(OAc)_4$/PVAc composite fibers; b) SEM image of Zn_2SnO_4 fibers calcined at 500 °C; c) cross-sectional view of Zn_2SnO_4 fibers calcined at 500 °C; d) Zn_2SnO_4 fibers calcined at 700 °C (reference); e) hot-pressed $Zn(OAc)_2$-$Sn(OAc)_4$/PVAc composite fibers; f) SEM image of Zn_2SnO_4 fibers calcined at 450 °C after hot-pressing step; g) cross-sectional view of Zn_2SnO_4 fibers calcined at 450 °C after hot-pressing step; h) TEM image of Zn_2SnO_4 fibers calcined at 450 °C after hot-pressing step; i) magnified TEM image in (h); j) magnified TEM image of (i) and the inset shows the SAED patten; k) X-ray diffraction pattern of Zn_2SnO_4 fibers calcined at various temperatures of 450 °C, 600 °C, and 700 °C.

porous (Figure 4i) and that the length of the Zn_2SnO_4 fibers can reach tens of micrometers. The inset image of Figure 4j shows that an individual Zn_2SnO_4 fiber has ring diffraction patterns of an amorphous structure with no sharp peak features. HR-TEM images of Zn_2SnO_4 fiber showed no crystalline lattice fringe, indicating an amorphous structure. This is in a good agreement with the XRD analysis. Figure 4k shows the X-ray diffraction (XRD) pattern of Zn_2SnO_4 fiber after calcination at various temperatures from 450 °C to 700 °C for 1 h. The XRD spectra show that the Zn_2SnO_4 fibers calcined at 450 °C have an amorphous structure. One broad peak was observed at around 34°, which originated from the amorphous Zn_2SnO_4 fibers, and noticeable sharp crystalline peaks were not found, confirming noncrystalline nature. Until up to 600 °C calcination, amorphous nature was maintained. After calcination at 700 °C, characteristic peaks, i.e., (220), (311), (220), (400), (422) and (511), of crystalline zinc stannate were clearly observed. Considering stable processing temperature limitation of FTO-coated glass substrate and optimized microstructures possessing fiber networks with high porosity and small particle sizes, we utilized amorphous-like Zn_2SnO_4 fibers calcined at 450 °C as a photoelectrode for application in DSSCs.

2.3. Photovoltaic Performance of DSSCs

In order to highlight the impact of the higher molar extinction coefficient of the organic sensitizers, we have fabricated

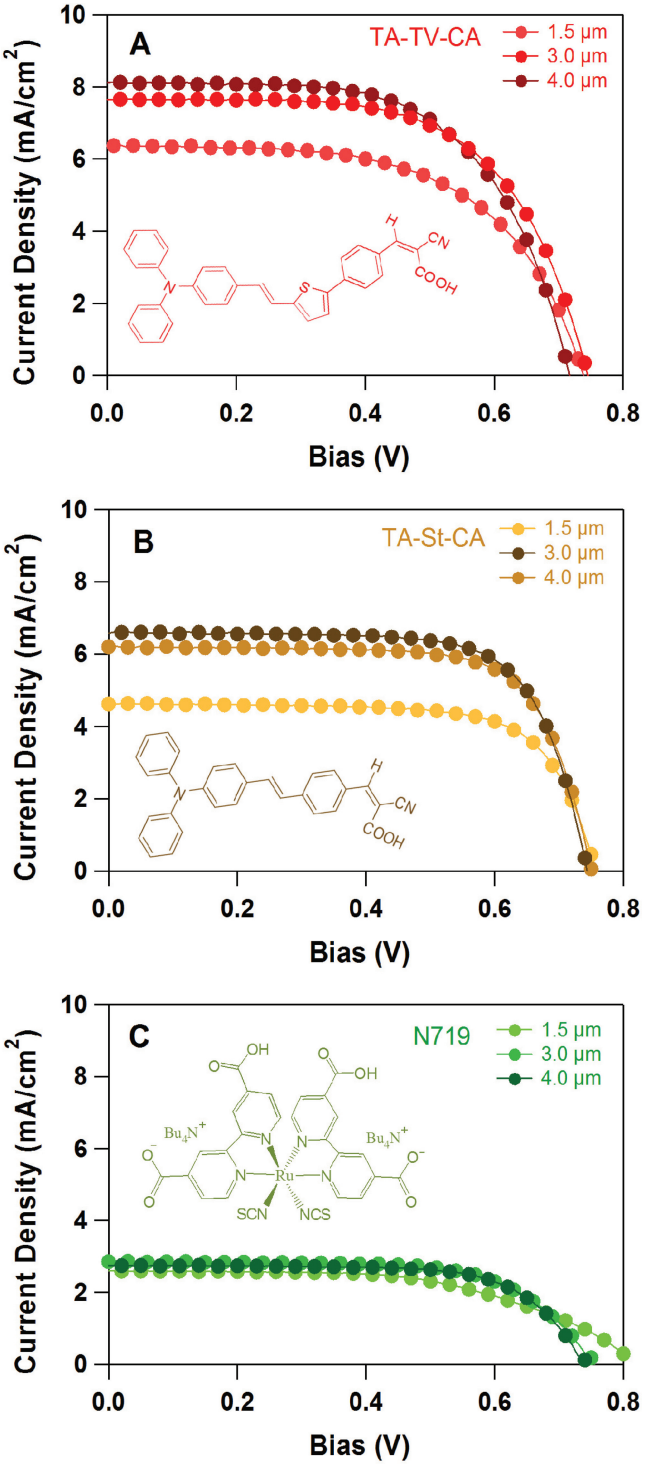

Figure 5. Photocurrent density-voltage (*J–V*) curves of DSSCs based on Zn_2SnO_4 photoelectrode and various sensitizers (TA-St-CA, TA-TV-CA and N719) under AM 1.5G irradiation (100 mW cm^{-2}), active area 0.40 cm^2.

DSSCs varying the thickness of Zn_2SnO_4 fiber photoelectrodes (1.5 μm, 3 μm and 4 μm). The organic dyes, TA-St-CA and TA-TV-CA, were sensitized with a conventional co-adsorbent, chenodeoxycholic acid (CDCA), to prevent undesirable aggregation on the electrode surface. The optimized conditions for the sensitization of the Zn_2SnO_4 electrodes employing these dyes are determined to be 1:1 ratio of dye/CDCA (5×10^{-4} M/5×10^{-4} M). N719 ruthenium based dye was used as a reference dye to evaluate the performances of the organic dyes. The dye sensitization time was 14 hours for all cells. DSSCs were fabricated using a conventional liquid electrolyte with 0.7 M 1-methyl-3-*n*-propylimidazolium iodide/0.1 M LiI/0.03 M I_2/0.5 M 4-*tert*-butylpyridine in a mixture of acetonitrile and valeronitrile (85/15, V/V). The typical active area of the cells was about 0.40 cm^2. The current density-voltage (*J–V*) characteristics of Zn_2SnO_4 fiber based DSSCs sensitized with a range of dyes were shown in **Figure 5**, where open-circuit photovoltage (V_{oc}), short-circuit photocurrent density (J_{sc}), fill factor (FF), and PCEs can be obtained. The measurement was performed under simulated AM 1.5G irradiation (100 mW cm^{-2}, one sun condition). Direct comparison of the DSSCs performance conducted on the same thicknesses for the electrodes demonstrate clearly higher efficiency by organic dyes. Even for the lowest thickness of Zn_2SnO_4 layer (1.5 μm) our new organic dye TA-TV-CA produced PCE of 2.77% (J_{sc} = 6.39 mA cm^{-2}, V_{oc} = 0.73 V and FF = 0.58). DSSCs using both organic dyes exhibited similar V_{oc} and FF values; however the TA-TV-CA based cells demonstrated a much higher J_{sc}. This result is due the enhanced light harvesting by TA-TV-CA since its absorption spectrum is red-shifted towards the visible and its molar extinction coefficient is higher than the one of TA-St-CA. The values from the *J–V* characteristic measurements of DSSCs are listed in **Table 2**.

The incident photon to current efficiency (IPCE) analysis results of DSSCs sensitized with a range of dyes, are plotted as a function of excitation wavelengths in **Figure 6**. High plateau was obtained on the IPCE spectrum of TA-TV-CA based cells, and it was red-shifted ≈25 nm compared to that of TA-St-CA based cell. This result is coincident with the result of absorption spectra of the organic dyes. The maximum IPCE of the TA-TV-CA was 62% at 450 nm, while that of TA-St-CA was 65% at 420 nm. The IPCE of N719 was significantly lower than that of the organic dyes, when the identical photoelectrode thickness was used, although it spread in a wider wavelength than that of organic dyes. The maximum IPCE of N719 was 17% at 550 nm. This reduced IPCE is attributed to the lower molar extinction coefficient of this dye. By increasing the thickness of

Table 2. Current-voltage (*J–V*) characteristics for DSSCs based on the organic dyes TA-St-CA, TA-TV-CA, and the reference dye N719.

Thickness of Zn_2SnO_4 photoelectrode	Dye	J_{sc} [$mAcm^{-2}$]	V_{oc} [mV]	FF [%]	PCE [%]
1.5 μm	TA-St-CA	4.62	756	71.0	2.48
	TA-TV-CA	6.39	728	58.6	2.77
	N719	2.59	818	55.3	1.17
3.0 μm	TA-St-CA	6.20	750	71.9	3.35
	TA-TV-CA	8.11	717	63.2	3.67
	N719	2.85	756	65.7	1.41
4.0 μm	TA-St-CA	6.57	744	71.7	3.50
	TA-TV-CA	7.66	745	62.3	3.55
	N719	2.75	744	68.6	1.40

the Zn_2SnO_4 electrodes, we observed an overall performance enhancement of the DSSCs for all dyes. While the performance improvement of N719 based cells was moderate, the photo-conversion efficiency (PCE) of the organic dyes based cells reached to 3.67% for TA-TV-CA on 3 µm-thick electrodes (J_{sc} = 8.11 mA cm^{-2}, V_{oc} = 0.72 V and FF = 0.63), and 3.50% for TA-TV-CA on 4 µm-thick electrodes (J_{sc} = 6.57 mA cm^{-2}, V_{oc} = 0.74V and FF = 0.72). It should be noted that the performance of the organic dyes were significantly higher compared to the ruthenium based dye N719 in our Zn_2SnO_4 photoelectrode based cells. The incorporation of additional thiophene unit in the chemical structure of the organic dye allows for 16 to 38% improvement of the current densities delivered by the cells in all the electrode thickness we tested. The thiophene-containing dye, TA-TV-CA, showed consistently enhanced performances compared to TA-St-CA for a given thickness of Zn_2SnO_4 photoelectrodes.

The efficiency of circa 3.7% at 1 sun for the TA-TV-CA sensitized Zn_2SnO_4 cell (with an electrode thickness of 3 µm) ranks among the highest efficiencies reported for Zn_2SnO_4 (up to 4.7%)[10d] and ZnO (up to 5%)[20] and for SnO_2 (up to 3.1%)[6] fabricated under hydrothermal conditions. Besides it should be underlined that all these records were obtained using electrodes showing higher thicknesses ranging from 10 µm to 14 µm.

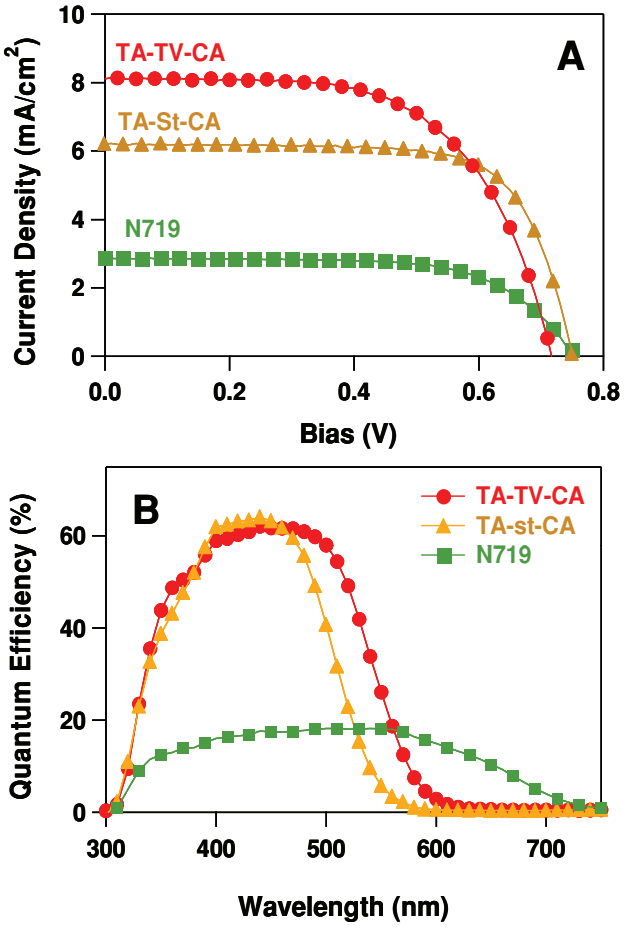

Figure 6. A) *J–V* curves and B) IPCE spectra for DSSCs based on Zn_2SnO_4 photoelectrode and various sensitizers.

The enhanced J_{sc} and IPCEs of organic dyes compared to N719 were further characterized in terms of dye-uptake using Langmuir adsorption isotherm plot.[21] To study the dye-loading process, UV-vis absorption spectra of the three dyes adsorbed on Zn_2SnO_4 nanofibers were acquired. The amount of adsorbed dye can be calculated using the extinction coefficient of the TA-St-CA, TA-TV-CA and N719 dye (3.6×10^7, 4.5×10^7 and 1.4×10^7 mol^{-1} cm^2 at the wavelength of 407, 427 and 535 nm, respectively). **Figure 7** shows the plots for the absorbance versus the dye loading time, and the corresponding dye adsorption amount that is represented by the right y-axis in the graphs. The dye molecules are absorbed rapidly in a few hours, and then the adsorption process slowed down afterward reaching saturation. Both organic dyes displayed much higher saturated dye-loading level (>13×10^{-9} mol cm^{-2}) than N719 (≈8×10^{-9} mol cm^{-2}) revealing another cause of enhanced J_{SC} in the organic dyes based cells (Figure 7). The adsorption process can be described using the following equation where θ is the dye coverage, κ represents the reaction constant, and n is the reaction order.[22]

$$-\frac{d(1-\theta)}{dt} = k(1-\theta)^n \quad (1)$$

We fitted the adsorption data using equation 1 with different reaction orders of n = 0, 1, and 2 and found that it could be best represented as a first-order reaction. The inset in Figure 7 shows the fitting result with n = 1, where ln(1– θ) exhibited a linear dependence on the dye loading time t. From this fitting the reaction constant κ could be calculated, which was 0.015 min^{-1} for TA-St-CA, 0.015 min^{-1} for TA-TV-CA and 0.004 min^{-1} for N719 dye, respectively.

3. Conclusion

We have reported the preparation of thin porous amorphous Zn_2SnO_4 fiber-based photoelectrodes via electrospinning. The surface and inner morphologies of the fibers are highly porous and smooth, with high specific surface area of 124 m^2 g^{-1}. Three different sensitizers, two donor-conjugate-acceptor (D-π-A) structured organic dyes and a ruthenium complex (N719) dye were used for the fabrication of Zn_2SnO_4 fiber-based DSSCs and their performances were investigated. Among the two organic sensitizers, the compound TA-TV-CA was specifically designed and synthesized to show a broader and higher absorption spectrum compared to its analog TA-St-CA. Remarkably, organic dye sensitized DSSCs displayed significantly improved performance (≈2.5 times higher) than that of the N719 sensitized DSSCs. The best performances for the cells were obtained using the new dye TA-TV-CA as sensitizer and reach 3.67% on a 3 µm-thick Zn_2SnO_4 electrode. This work highlights the potential of amorphous Zn_2SnO_4 electrodes for the development of efficient organic sensitized DSSCs and offer future perspective for the development of solid state DSSCs.

4. Experimental Section

Preparation of Zn_2SnO_4 Nanofibers Mat Films: Poly(vinyl acetate) (PVAc, M_w = 1 300 000 mol g^{-1}) was synthesized using bulk radical polymerization. $Zn(CH_3COO)_2{\cdot}2H_2O$ (99%+) and $Sn(CH_3COO)_4$

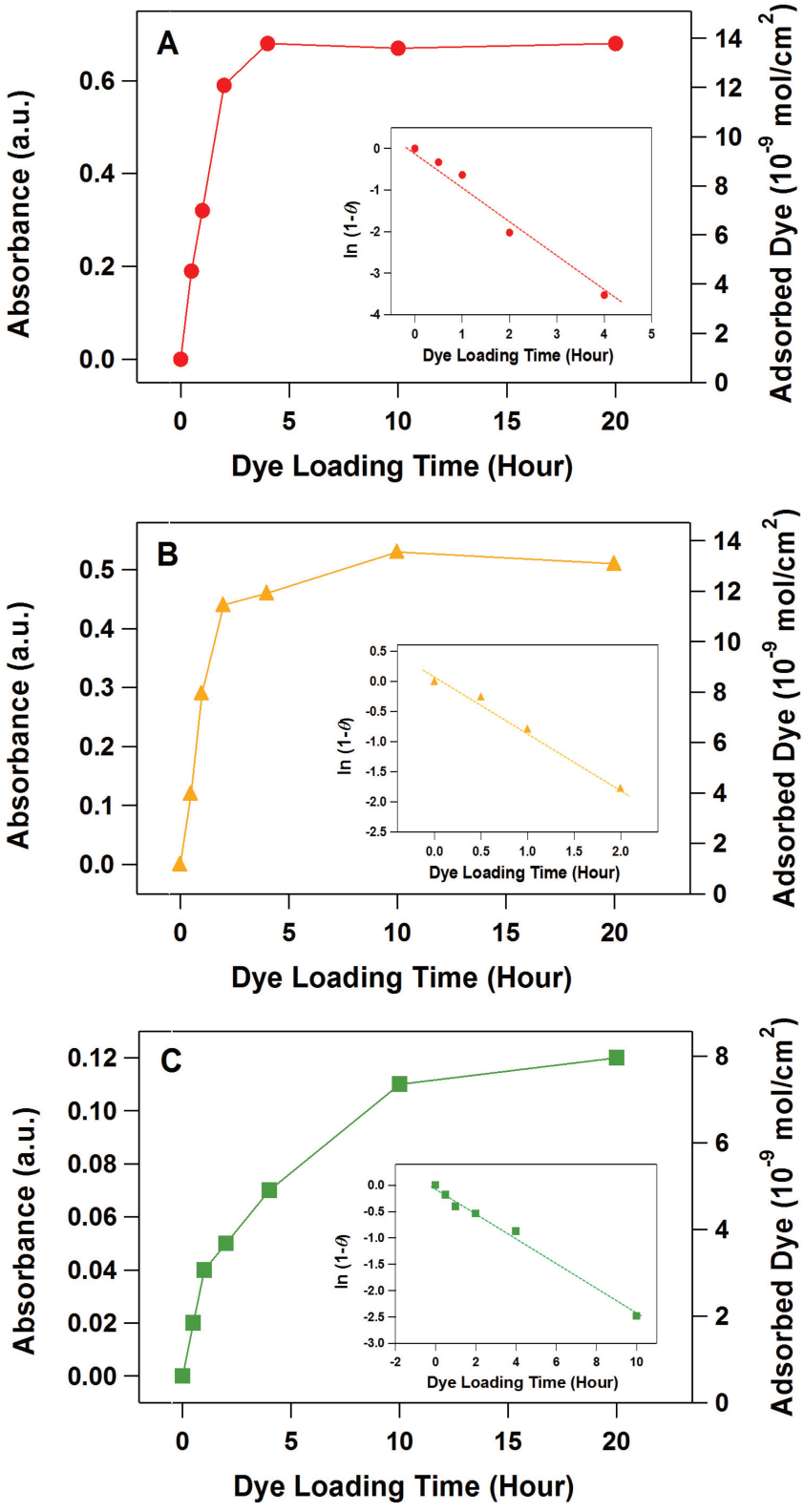

Figure 7. Absorbance of A) TA-St-CA, B) TA-TV-CA and C)N719 dye as a function of dye loading time. The corresponding amount of the adsorbed dye molecules is also given by the right *y*-axis. Insets show the fitted adsorption rate (k) equation for a first-order reaction. The thickness of the Zn_2SnO_4 fiber photoelectrodes was 3 µm.

(99%+) were purchased from Aldrich. Anhydrous N,N-dimethylformamide (DMF) was obtained from J.T Baker. The chemical reagents were used without further purification. For the synthesis of zinc tin oxide fibers, the precursor solution for electrospinning was prepared by dissolving 1.756 g of $Zn(CH_3COO)_2{\cdot}2H_2O$ ($Zn(OAc)_2$), 1.420 g of $Sn(CH_3COO)_4$ ($Sn(OAc)_4$) and 1.500 g of PVAc in DMF (15.8 mL). During the electrospinning process the solution was injected through a stainless steel needle (25 gauge, orifice diameter = 250 µm) that was connected to a high-voltage DC power supply (Bertan, High-voltage power supply series 230). The solution was continuously fed through the nozzle using a syringe pump (KD scientific, 781200) at a rate of 20 µL min^{-1}. High voltage (17.2 kV) was applied between the needle and the grounded collector, located 15 cm below the needle. The precursor solution was directly electrospun on F:SnO_2 (FTO) coated glass. The as-spun $Zn(OAc)_2$, $Sn(OAc)_4$/PVAc composite fiber mats were then pressed using preheated metallic plates at 120 °C for 5 min. A 1 cm thick Teflon plate was inserted between the $Zn(OAc)_2$-$Sn(OAc)_4$/PVAc composite fiber mats and the plate to apply a uniform pressure (120 kg cm^{-2}) and prevent sticking of the fibers to the plate. Subsequently, the samples were calcined at 450 °C for 1 h in air.

Characterization of the Zn_2SnO_4 Nanofibers Mat Films: The morphology and microstructural evolution were examined by field emission scanning electron microscopy (FE-SEM, JEOL JSM 6330F). A focused ion beam (FIB, NOVA 600, FEI) was used to cut sharp cross sections of the Zn_2SnO_4 fibers or mats calcined at 450 °C for closer examination of their inner morphology. High-resolution TEM (HR-TEM, Tecnai G2 (FEI)) were used for the microstructural analyses of the prepared fibers. Thermogravimetric studies were carried out using a TG-2050 thermal analyzer system (Ta instruments, Inc.). X-ray diffraction (XRD) was used to examine the phase composition of Zn_2SnO_4 fiber mats. The surface areas of the Zn_2SnO_4 fibers were investigated using the Brunauer-Emmett-Teller (BET) method (Belsorpmini, BEL Lapan Inc.).

Synthesis of the Dye TA-TV-CA: *N,N*-Diphenylaminobenzaldehyde,4-bromobenzaldehyde, 2-cyanoacetic acid, di-*tert*-butyl-*p*-cresol, piperidine, pyridine, potassium *tert*-butoxide (1.0 M solution in tetrahydrofuran (THF)), methyltriphenylphosphonium were purchased from Aldrich or TCI chemicals and used as received. 4-(thien-2-yl)benzaldehyde and N-Bromo-Succinimide (NBS) were purchased from Fisher Chemicals. The solvents, such as absolute methanol, *N,N*-dimethyl-formamide (DMF), *N,N*-dimethylacetamide (DMAc), and acetonitrile from Aldrich were used as received. THF was used after distillation under sodium and benzophenone. Spectroscopic grade solvents from Aldrich were used for spectral measurements. *N,N*-diphenyl-4-vinylaniline (TA-Vinyl) was synthesized according to reference 16. Alternatively the precursors and the organic dyes could be purchased from Kaïronkem (http://www.kaironkem.com/).

Synthesis of 4-(5-Bromothiophen-2-yl)-benzaldehyde (1): In a two-neck flask, 0.750 g (3.98 mmol) of

4-(thien-2-yl)benzaldehyde were introduced and solubilized in 20 mL of DMF. The mixture was cooled to 0 °C. Then 0.780 g (1,1 eq., 4.38 mmol) of *N*-bromosuccinimide solubilized in a mixture of 10 mL of DMF and 10 mL of methanol were added dropwise over 30 min in the dark. The resulting mixture was allowed to warm up to room temperature and stirred for two hours. The reaction was then hydrolyzed using HCl aqueous solution (1M) and then it was extracted using diethylether (50 mL). Organic phase was washed with brine and dried over Na_2SO_4. After filtration and evaporation of the solvent, the product was crystallized from acetone to yield 0,750 g of a white solid (yield: 70.6%). ^{1}H NMR (200 MHz, $CDCl_3$-*d*, δ): 7.10 (dd, 1H, J = 4.0 Hz, J = 0.5 Hz), 7.20 (dd, 1H, J = 3.9 Hz, J = 0.5 Hz), 7.66 (d, 2H, J = 8.3 Hz), 7.88 (d, 2H, J = 8.2 Hz), 10.00 (s, 1H).

Synthesis of 4-(5-(4-(Diphenylamino)styryl)thiophen-2-yl)-benzaldehyde (2): In a three-neck flask, 0.750 g (2.81 mmol) of (**1**), 27 mg (1% molar) of trans-di(μ-acetato)bis[o-(di-o-tolylphosphino)benzyl] dipalladium(II), 124 mg (20% molar) of 2,6-di-*tert*-butylcresol and 0.655 g (2.2 eq) of sodium carbonate were dissolved in 15 mL of DMAC under argon. The mixture was heated at 90 °C. Then 1.520 g of TA-Vinyl (2 eq.) solubilized in 15 mL were added. After addition the mixture was heated at 135 °C and stirred during 24 h. The mixture was allowed to cool to room temperature and then 100 mL of deionized water were added followed by 100 mL of CH_2Cl_2. The organic phase was separated and washed with 100 mL of HCl aqueous solution (2 M) and 100 mL of brine. Then the organic phase was dried over Na_2SO_4. After filtration and evaporation of the solvent, the raw product was purified by column chromatography on silica gel using a mixture of hexane and ethyl acetate as eluent (95/5, v/v). The product was obtained as an orange solid. (0.520 g, yield: 40.5%). ^{1}H NMR (200 MHz, $CDCl_3$-*d*, δ): 7.08 (m, 10H), 7.35 (m, 6H), 7.52 (d, 1H, J = 8.58 Hz), 7.72 (d, 1H, J = 3.81 Hz), 7.92 (q, 4H), 10.00 (s, 1H).

Synthesis of 2-Cyano-3-(4-(5-(4(diphenylamino)styryl)thiophen-2-yl) phenyl)acrylic Acid (TA-TV-CA): The product was prepared using Knoevenagel condensation conditions. In a two-neck flask 0.395 g (0.863 mmol) of (2) and 1.470g (20 eq.) of cyano-acrylic acid were dissolved in acetonitrile under argon. Few drops of pyridine were added to the mixture and the mixture was refluxed during 2 h. After cooling to room temperature, the solvent was removed under vacuum and the crude product was dissolved in chloroform (50 mL) then washed with 100 mL of HCl aqueous solution (2 M) and 100 mL of water. The organic phase was dried over Na_2SO_4, filtered and concentrated under vacuum. The product was precipitated from hexane and recrystallized from THF-hexane. After filtration the product was dried in an oven to yield 0.305 g of a dark brown solid (yield: 69.6%). RMN ^{1}H (DMSO-d_6, δ): 7.10 (m, 9H), 7.35 (m, 6H), 7.52 (d, 2H, J = 8.68 Hz), 7.74 (d, 1H, J = 3.84 Hz), 7.91 (d, 2H, J = 8.48 Hz), 8.10 (d, 2H, J = 8.66 Hz), 13.98 (s, 1H). UV-vis (Ethanol): λ_{max} (ε) = 427 nm (44600). Anal. Calcd for $C_{34}H_{24}N_2O_2S$: C 77.84, H 4.61, N 5.34, S 6.11; found: C 77.54, H 4.57, N 5.28, S 5.98.

Characterization of the Dyes: UV-vis absorption spectra were recorded in solution on a Perkin-Elmer Lambda 2 spectrometer (wavelength range: 180–820 nm; resolution: 2 nm). Electrochemical studies of the synthesized molecules were carried out in a one compartment, three-electrode electrochemical cell equipped with a flat platinum working electrode (7 mm^2), a Pt wire counter electrode, and a Ag wire pseudo-reference electrode, whose potential was checked using the Fc/Fc^+ couple as an internal standard. The electrolyte consisted of 0.1 M tetrabutylammonium tetrafluoroborate (Bu_4NBF_4) solution in dichloromethane containing 1 to 2×10^{-3} M of the dyes (depending on the solubility). The experiments were carried out in a glove box.

Device Fabrication: The Zn_2SnO_4 fibers mat films were rinsed with ethanol and then sintered at 500 °C for 30 min. After cooling to 80 °C, the Zn_2SnO_4 electrodes were immersed for 15 h at room temperature into ethanol solution containing 3×10^{-3} M chenodeoxycholic acid (CDCA) and 3×10^{-4} M of *cis*-di(thiocyanato)-*N,N'*-bis(2,2'-bipyridyl-4-carboxylic acid-4'-tetrabutyl ammonium carboxylate) ruthenium(II) (N719, Solaronix), or TA-St-CA, or TA-TV-CA). For the counter electrode, the FTO plates were drilled by a microdrill, washed with 0.1 M HCl solution in ethanol, and then subsequently cleaned in an ultrasonic bath with water and ethanol for 15min. A Pt counter electrode was prepared by drop casting of 5 mM H_2PtCl_6 in isopropyl alcohol onto the washed FTO plates and then sintered at 400 °C for 20 min under air conditions. The dye-adsorbed Zn_2SnO_4 electrodes were rinsed with ethanol and dried under nitrogen flow. Then they were assembled and sealed with the counter electrode using the thermal adhesive films (Surlyn, Dupont 1702, 25-μm-thick) as a spacer to produce sandwich-type cells. The liquid electrolyte consisted of 0.7 M 1-propyl-3-methylimmidazolium iodide, 0.03 M iodine, 0.1 M lithium iodide and 0.5 M 4-*tert*-butylpyridine in a mixture of acetonitrile and valeronitrile (85/15 v/v). An electrolyte solution was introduced through a drilled hole on the counter electrode. Finally, the holes were sealed with a hot-melt films and a cover glass. The active area of cell was about 0.40 cm^2.

Dye Uptake: The annealed Zn_2SnO_4 films were sensitized with 3×10^{-3} M chenodeoxycholic acid (CDCA) and N719 dye, TA-St-CA, or TA-TV-CA, respectively. The amount of the adsorbed dye was monitored as a function of time. The adsorbed dye was quantitatively determined from the absorbance at 407, 427 and 535 nm measured by UV-vis spectrophotometer, where dyes were desorbed by immersing the dye-covered Zn_2SnO_4 films in 10 mL of 0.1 M NaOH aqueous solution for 10 min.

Computational Details: The density functional theory (DFT) calculations were performed on the two organic sensitizers by using the Amsterdam Density Functional package (ADF 2010.01).[23,24] The structures of the dyes have been fully optimized at a GGA level using the Perdew-Burke-Ernzerhof (PBE) functional and triple zeta plus 2 polarization Slater functions (TZ2P set in ADF) basis sets for all atoms, with 1s orbitals frozen for C, N and O atoms. On these optimized geometries, B3LYP hybrid functional calculations with TZ2P all electron basis sets were then performed to yield more reliable frontier orbital energies. Acetonitrile solvent was taken into account using a polarizable continuum model (COSMO in ADF)[25] for all geometry optimizations and B3LYP single point calculations. Orbitals were drawn using the graphical interface of ADF (ADF-GUI).[23]

Photovoltaic and Photoelectrical Measurements: Photovoltaic measurement of the DSSCs employed an AM 1.5 solar simulator between the sample and a 450 W Xe lamp. The intensity of the simulated light was calibrated by a Si reference solar cell equipped with a KG5 filter for approximating AM 1.5 global radiation. The photovoltaic characteristics of DSC were obtained by applying an external potential bias to the cells and measuring the generated photocurrent with a Keithley model 2400 source meter. IPCE was measured as a function of wavelength from 300 nm to 800 nm using a specially designed IPCE system for dye-sensitized solar cell (PV measurement, Inc.). A 75 W xenon lamp was used as the light source for generating a monochromatic beam. Calibration was performed using a NIST-calibrated silicon photodiode as a standard. IPCE values were collected at a low chopping speed of 4Hz. The electrical impedance spectra were measured using an impedance analyzer (Solartron 1260) at an open-circuit potential under AM 1.5 full sun illumination (100 mW cm^{-2}), with a frequency range of 0.1–10^5 Hz. The magnitude of the alternative signal was 10 mV. Impedance parameters were determined by fitting of the impedance spectra using Z-plot software.

Supporting Information

Supporting Information is available from the Wiley Online Library or from the author.

Acknowledgements

S.-H.C. and D.H. contributed equally to this work. R.D. and I.D.K. acknowledge CEA and KIST for initiating this collaboration through

the Nanosciences Research Program. S.Y.J. gratefully acknowledge support from the Basic Science Research Program through the National Research Foundation of Korea (NRF, 2012045675), funded by the Ministry of Education, Science. Acknowledgment is made to the Campus France and Egide for partial financial support of this research through the STAR research program (Grant number 21443NJ). R.D. thanks Dr. D. Aldakov for helpful discussions. I.D.K. acknowledges the support by the Engineering Research Center (ERC-N01120073) program from the Korean National Research Foundation.

Received: November 8, 2012
Revised: December 10, 2012
Published online: February 6, 2013

[1] B. O'Regan, M. Graetzel, *Nature* **1991**, *353*, 737.
[2] a) *Dye-sensitized Solar Cells, 1st ed.*, (Ed: K. Kalyanasundaram), EPFL Press, Lausanne, Switzerland, **2010**; b) A. Hagfeldt, G. Boschloo, L. Sun, L. Kloo, H. Pettersson, *Chem. Rev.* **2010**, *110*, 6595; c) M. K. Nazeeruddin, P. Pechy, T. Renouard, S. M. Zakeeruddin, R. Humphry-Baker, P. Comte, P. Liska, L. Cevey, E. Costa, V. Shklover, L. Spiccia, G. B. Deacon, C. A. Bignozzi, M. Grätzel, *J. Am. Chem. Soc.* **2001**, *123*, 1613; d) A. Yella, H-W Lee, H. N. Tsao, C. Yi, A. K. Chandiran, Md.K. Nazeeruddin, E.W-G. Diau, C-Y Yeh, S.M. Zakeeruddin, M. Grätzel, *Science* **2011**, *334*, 629.
[3] a) M. K. Nazeeruddin, F. D. Angelis, S. Fantacci, A. Selloni, G. Viscardi, P. Liska, S. Ito, B. Takeru, M. Grätzel, *J. Am. Chem. Soc.* **2005**, *127*, 16835; b) A. Mishra, M. K. R. Fischer, P. Bäuerle, *Angew. Chem.* **2009**, *121*, 2510; *Angew. Chem. Int. Ed.* **2009**, *48*, 2474; c) Z. J. Ning, Y. Fu, H. Tian, *Energy Environ. Sci.* **2010**, *3*, 1170; d) F. Gao, Y.Wang, D. Shi, J. Zhang, M. Wang, X. Jing, R. Humphry-Baker, P. Wang, S.M. Zakeeruddin, M. Grätzel, *J. Am. Chem. Soc.* **2008**, *130*, 10720; e) A. Mishra, N. Pootrakulchote, M. K. R. Fischer, C. Klein, Md. K. Nazeeruddin, S.M. Zakeeruddin, P. Bauerle, M. Graetzel, *Chem. Commun.* **2009**, 7146; f) B. E. Hardin, H. J. Snaith, M. D. McGehee, *Nat. Photonics* **2012**, *6*, 162; g) A. Nattestad, A. J. Mosser, M. K. R. Fischer, Y.-B. Cheng, A. Mishra, P. Bäuerle, U. Bach, *Nat. Mater.* **2010**, *9*, 31.
[4] a) M. Graetzel, *J. Photochem. Photobiol. A* **2004**, *164*, 1; b) Y. Chiba, A. Islam, Y. Watanabe, R. Komiya, N. Koide, L. Han, *Jpn. J. Appl. Phys. 2* **2006**, *45*, 24, L638; c) G. K. Mor, K. Shankar, M. Paulose, O.K. Varghese, C.A. Grimes, *Nano. Lett.* **2006**, *6*, 215.
[5] a) M. Quintana, T. Edvinsson, A. Hagfeldt, G. Boschloo, *J. Phys. Chem. C* **2007**, *111*, 1035; b) K. Keis, E. Magnusson, H. Lindstrom, S-E. Lindquist, A. Hagfeldt, *Sol. Energy Mater. Sol. Cells* **2002**, *73*, 51; c) M. Law, L.E. Greene, J.C. Johnson, R. Saykally, P. Yang, *Nat. Mater.* **2005**, *4*, 455; d) A. B. F. Martinson, J.E. McGarrah, M.O.K. Parpia, J.T. Hupp, *Phys. Chem. Chem. Phys.* **2006**, *8*, 4655.
[6] a) A. Kay, M. Grätzel, *Chem. Mater.* **2002**, *14*, 2930; b) E. N. Kumar, R. Jose, P.S. Archana, C. Vijila, M.M. Yusoff, S. Ramakrishna, *Energy Environ. Sci.* **2012**, *5*, 5401; c) Y. P. Y. P. Ariyasinghe, T. R. C. K. Wijayarathna, I. G. C. K. Kumara, I. P. L. Jayarathna, C. A. Thotawatthage, W. S. S. Gunathilake, G. K. R. Senadeera, V. P. S. Perera, *J. Photochem. Photobiol. A* **2011**, *217*, 249.
[7] a) P. Guo, M. A. Aegerter, *Thin Solid Films* **1999**, *351*, 290; b) K. Sayama, H. Sugihara, H. Arakawa, *Chem. Mater.* **1998**, *10*, 3825.
[8] K. Hara, T. Horiguchi, T. Kinoshita, K. Sayama, H. Sugihara, H. Arakawa, *Sol. Energy Mater. Sol. Cells* **2000**, *64*, 115.
[9] S. Burnside, J.E. Moser, K. Brooks, M. Graetzel, D. Cahen, *J. Phys. Chem. B* **1999**, *103*, 9328.
[10] a) B. Tan, E. Toman, Y. Li, Y. Wu, *J. Am. Chem. Soc.* **2007**, *129*, 4162; b) Z. Li, Y. Zhou, C. Bao, G. Xue, J. Zhang, T. Yu, Z. Zou, *Nanoscale* **2012**, *4*, 3490; c) L. Huang, L. Jiang, M. Wei, *Electrochem. Commun.* **2010**, *12*, 319; d) D-W. Kim, S-S. Shin, I-S Cho, S. Lee, D-H. Kim, C-W. Lee, H-S. Jung, K-S Hong, *Nanoscale* **2012**, *4*; 557.
[11] T. J. Coutts, D. L. Young, X. Li, W. P. Mulligan, X. Wu, *J. Vac. Sci. Technol. A.* **2000**, *18*, 2646.
[12] M. A. Alpuche-Aviles, Y. Wu, *J. Am. Chem. Soc.* **2009**, *131*, 3216.
[13] a) M. Graetzel, *Inorg. Chem.* **2005**, *44*, 6841; b) N. Robertson, *Angew. Chem.* **2006**, *118*, 2398; *Angew. Chem. Int. Ed.* **2006**, *45*, 2338; c) P. Xie, F. Guo, *Curr. Org. Chem.* **2007**, *11*, 1272; d) F.-T. Kong, S.-Y. Dai, K.-J. Wang, *Adv. Opt. Electron.* **2007**, 75384; e) J. M. Kroon, N. J. Bakker, H. J. P. Smit, P. Liska, K. R. Thampi, P.Wang, S. M. Zakeeruddin, M. Graetzel, A. Hinsch, S. Hore, U.Wurfel, R. Sastrawan, J. R. Durrant, E. Palomares, H. Pettersson, T. Gruszecki, J. Walter, K. Skupien, G. Tulloch, *Prog. Photovoltaics* **2007**, *15*, 1.
[14] C-Y. Chen, M Wang, J-Y Li, N. Pootrakulchote, L. Alibabaei, C. Ngoc-le, J-D Decoppet, J-H. Tsai, C. Graetzel, C-G Wu, S. M. Zakeeruddin, M Grätzel, *ACS Nano* **2009**, *3*, 3103.
[15] a) A. Mishra, M. K. R. Fischer, P. Bauerle, *Angew. Chem. Int. Ed* **2009**, *48*, 2474; b) T-H. Kwon, V. Armel, A. Nattestad, D. R. MacFarlane, U. Bach, S. J. Lind, K. C. Gordon, W. Tang, D. J. Jones, A. B. Holmes, *J. Org. Chem.* **2011**, *76*, 4088.
[16] a) S. Hwang, J. H. Lee, C. Park, H. Lee, C. Kim, C. Park, M.-H. Lee, W. Lee, J. Park, K. Kim, N.-G. Park, C. Kim, *Chem. Commun.* **2007**, *46*, 4887; b) G-W Lee, D. Kim, M. J. Koa, K. Kim, N-G. Park, *Sol. Energy* **2010**, *84*, 418.
[17] J. Bouclé, J. Ackermann, *Polym. Int.* **2012**; *61*, 355.
[18] F. Gao, Y. Wang, D. Shi, J. Zhang, M. Wang, X. Jing, R. Humphry-Baker, P. Wang, S. M. Zakeeruddin, M. Grätzel, *J. Am. Chem. Soc.* **2008**, *130*, 10720.
[19] S-H. Choi, I-S. Hwang, J-H. Lee, S-G. Oh, I-D. Kim, *Chem. Commun.* **2011**, *47*, 9315.
[20] a) K. Kakiuchi, E. Hosono, S. Fujihara, *J. Photochem. Photobiol. A* **2006**, *179*, 81; b) K. Keis, E. Magnusson, H. Lindstrom, S-E Lindquist, A. Hagfeldt, *Sol. Energy Mater. Sol. Cells* **2002**, *73*, 51
[21] K.-J. Hwang, W.-G. Shim, S.-H. Jung, S.-J. Yoo, J.-W Lee, *Appl. Surf. Sci.* **2010**, *256*, 5428.
[22] C.-R. Lee, H.-S. Kim, I.-H. Jang, J.-H. Im, N.-G. Park, *Appl. Mater. Interfaces* **2011**, *3*, 1953.
[23] ADF **2010**, SCM, Theoretical Chemistry, Vrije Universiteit, The Netherlands Amsterdam, http://www.scm.com (accessed October 2012).
[24] a) G. te Velde, F. M. Bickelhaupt, S. J. A. van Gisbergen, C. Fonseca Guerra, E. J. Baerends, J. G. Snijders, T. Ziegler, *J. Comput. Chem.* **2001** *22*, 931; b) Fonseca Guerra, J. G. Snijders, G. te Velde, E. J. Baerends, *Theor. Chem. Acc.* **1998**, *99*, 391.
[25] C. C. Pye, T. Ziegler, *Theor. Chem. Acc.* **1999**, *101*, 396.